Optimizing Privacy-Preserving Outsourced Convolutional Neural Network Predictions

Minghui Li, Sherman S. M. Chow, Shengshan Hu, Yuejing Yan, Chao Shen, and Qian Wang

Abstract—Convolutional neural network is a machine-learning model widely applied in various prediction tasks, such as computer vision and medical image analysis. Their great predictive power requires extensive computation, which encourages model owners to host the prediction service in a cloud platform. Recent researches focus on the privacy of the query and results, but they do not provide model privacy against the model-hosting server and may leak partial information about the results. Some of them further require frequent interactions with the querier or heavy computation overheads, which discourages querier from using the prediction service. This paper proposes a new scheme for privacy-preserving neural network prediction in the outsourced setting, *i.e.*, the server cannot learn the query, (intermediate) results, and the model. Similar to SecureML (S&P'17), a representative work that provides model privacy, we leverage two non-colluding servers with secret sharing and triplet generation to minimize the usage of heavyweight cryptography. Further, we adopt asynchronous computation to improve the throughput, and design garbled circuits for the non-polynomial activation function to keep the same accuracy as the underlying network (instead of approximating it). Our experiments on MNIST dataset show that our scheme achieves an average of $122\times$, $14.63\times$, and $36.69\times$ reduction in latency compared to SecureML, MiniONN (CCS'17), and EzPC (EuroS&P'19), respectively. For the communication costs, our scheme outperforms SecureML by $1.09\times$, MiniONN by $36.69\times$, and EzPC by $31.32\times$ on average. On the CIFAR dataset, our scheme achieves a lower latency by a factor of $7.14\times$ and $3.48\times$ compared to MiniONN and EzPC, respectively. Our scheme also provides $13.88\times$ and $77.46\times$ lower communication costs than MiniONN and EzPC on the CIFAR dataset.

Index Terms—Secure outsourcing, Machine learning, Convolutional neural network, Homomorphic encryption

✦

1 INTRODUCTION

MACHINE learning (ML) [1] performs well in many applications and has been widely used (*e.g.*, [2], [3], [4]). Neural networks, which identify relationships underlying a set of data by mimicking how the human brain operates, have recently gained extensive attention. Convolutional neural networks (CNN), based on biologically-inspired variants of multi-layer perceptrons, are proven to be useful in medical image analysis and recognition of images and videos.

With the popularity of machine-learning-as-a-service (MLaaS), the model owners tend to host the model in the cloud-based MLaaS for providing prediction services. Nevertheless, it is tempting for an adversary to steal the model [5], pirate it, or use it to provide a commercial prediction service for profits [6] since it is a valuable asset. Moreover, with the knowledge of the model, the risk of

- M. Li, and Q. Wang are with the School of Cyber Science and Engineering, School of Computer Science, Wuhan University, Wuhan 430072, Hubei, China, and State Key Laboratory of Cryptology, P.O. Box 5159, Beijing, 100878, China. E-mail: {minghuili, qianwang}@whu.edu.cn
- S. Chow is with the Department of Information Engineering, The Chinese University of Hong Kong, Hong Kong. E-mail: sherman@ie.cuhk.edu.hk
- S. Hu is with the Services Computing Technology and System Laboratory, Cluster and Grid Computing Laboratory, National Engineering Research Center for Big Data Technology and System, School of Cyber Science and Engineering, Huazhong University of Science and Technology, Wuhan 430074, Hubei, China. E-mail: hushengshan@hust.edu.cn
- Y. Yan is with State Key Laboratory of Information Engineering in Surveying, Mapping, and Remote Sensing, Wuhan University, Wuhan 430072, Hubei, China. E-mail: yjyan@whu.edu.cn
- C. Shen is with School of Cyber Security, School of Electronic and Information Engineering, Xi'an Jiaotong University, Xian 710049, Shaanxi, China. E-mail: cshen@sei.xjtu.edu.cn

compromising the model privacy is higher since white-box attacks can infer more information than black-box attacks, *e.g.*, membership inference attack [7], [8], [9] for determining if a specific sample was in the training dataset. Knowing the model also makes adversarial example attacks [10], [11], [12], [13] more effective. A tiny perturbation of the input can deceive the model and threaten its accuracy.

Outsourcing the model and the prediction service to any untrusted cloud platform (say, for relieving from the cost of maintaining an online server) thus comes with great privacy and security implications. This paper aims to propose an efficient prediction service that ensures *model privacy*, *i.e.*, keeping the model private from the querier (as most existing works) and any hosting server.

1.1 Related Work

Techniques in preserving privacy in neural network prediction can be broadly categorized into differential privacy, trusted processors, and cryptography. Differential privacy [14], [15] adds noise without sacrificing too much data utility, but it cannot ensure data privacy as much as the other two classes of techniques. Trusted processor (*e.g.*, SGX) approaches [16], [17], [18], [19], [20] work on the data within the trusted perimeter, but they are subjected to the memory constraint (currently 128MB) which can be easily exceeded by a specific layer of a deep neural network. Cryptographic approaches do not have these problems but with higher overheads. Ensuring privacy with a tailored cryptographic design is a recurrent research problem.

Many existing schemes protect the privacy of the *query* from the server. Yet, they consider the model owner is the

server performing the prediction tasks, *i.e.*, the prediction service only works with the *plaintext knowledge of the model*. Some works [21], [22] use additive homomorphic encryption to perform operations over the encrypted query and the clear model. Others [23], [24], [25], [26], [27] design secure two-party computation (S2C) protocols for various kinds of machine-learning computations. MiniONN [23] and Gazelle [24] adopted secret sharing in which the query is secret-shared (between the user) with the server. DeepSecure [25] preprocesses the data and the neural network before S2C but leaks some information about the parameters. XONN [26] "replaces" the matrix multiplication with XNOR, which is virtually free in GC. Yet, this scheme only applies to binary neural networks, *i.e.*, the parameters are binary. EzPC [27] proposes a compiler that translates between arithmetic and boolean circuits. However, the S2C-based approach often expects the queriers to remain online and interact with the server continuously, thus bringing some burden to the queriers and incurring higher network round-trip time.

Fully-homomorphic encryption (FHE) [28] allows processing (any polynomial functions over) encrypted data. It is thus a handy tool for not only processing the query in an encrypted format but also processing over an encrypted model. Bost *et al.* [29] considered various machine-learning classifications (*e.g.*, hyperplane decision-based classifiers, naïve Bayes classifiers, decision trees) over FHE-encrypted data. In the case of decision trees, Tai *et al.* [30] managed to use only additive HE instead of FHE to support S2C evaluation, but it is subject to the limitation that the server needs to know the model in clear. Using multi-key FHE, Aloufi *et al.* [31] considered secure outsourcing of decision-trees evaluation. The evaluation results can only be decrypted with the help of multiple secret keys from multiple parties. Chow [32] provided a brief overview of the state-of-the-art in privacy-preserving decision tree evaluation. All these works did not consider neural networks. Indeed, processing an FHE-encrypted neural network directly without optimization is time-consuming. FHE also fails to cover common non-polynomial operations in neural networks. CryptoDL [33] and E2DM [34] approximate them by polynomials, which degrades the prediction accuracy. A major drawback is that these approaches require the model owner to encrypt the model w.r.t the public key of each querier. It not only does not scale when there are multiple queriers, but also increases the risk of model leakage since any querier has the power to decrypt the model.

1.2 Two-Server Computation Model

To reduce the use of cryptographic techniques, many works [35], [36], [37], [38], [39] exploited the non-colluding assumption for the possibility of using lightweight cryptographic primitives, such as replacing the use of FHE with additive HE [37], [38]. SecureML [40] uses *additive secret sharing* [41] to share the model among two servers. The querier also secret-shares the query across the servers. To carry out prediction, the two servers interact with each other and eventually derive their corresponding share of the prediction result. The querier can then obtain the final

TABLE 1
Comparison of related work

	Privacy			Accuracy	Efficiency
	model para.	inter. data	query		
CryptoNets [21]	✗	✓	✓	Low	Medium
CryptoDL [33]	✓	✓	✓	Low	Medium
E2DM [34]	✓	✓	✓	Low	Medium
XONN [26]	✗	✓	✓	Medium	High
DeepSecure [25]	✗	✓	✓	High	Medium
SecureML [40]	✓	✓	✓	High	Medium
MiniONN [23]	✗	✓	✓	High	High
Gazelle [24]	✗	✓	✓	High	High
EzPC [27]	✗	✓	✓	High	High
Our Scheme	✓	✓	✓	High	High

result by merging both shares locally. The benefit of using secret sharing is that both servers can operate over the secret share, without knowing the underlying secret, almost as efficient as the operating over the secret itself. When the servers do not collude, none of the respective shares reveals anything about the secret.

To speed up the online (inner-product) computation, SecureML generates Beaver's multiplication *triplet* [42] for additive sharing in an offline preprocessing phase. For the non-polynomial operation (*i.e.*, comparison), they use Yao's garbled circuits (GC) [43] for boolean computations. Yet, SecureML only focuses on simple neural networks (and linear/logistic regression) without considering the more complex convolutional neural networks.

Looking ahead, our scheme follows this design and incorporates efficiency improvement over it. Fig. 1 overviews such a design, to be explained in Section 3.1.

Table 1 coarsely compares existing schemes. It is fair to say that there is no outsourcing solution with model privacy and satisfactory performance in accuracy and efficiency.

1.3 Our Contributions

proposes a new scheme that can simultaneously protect the query, the model, any intermediate results, and the final prediction results against the servers. Our contributions lie in maintaining high accuracy and efficiency, which are summarized below.

- We design protocols for different stages of the convolutional neural network prediction.
- We accelerate the triplets generation [40], [42] using single-instruction-multiple-data (SIMD) [44]. We also adopt asynchronous computation to speed up both offline and online computations.
- For non-polynomial activation functions, we design a series of garbled circuits for S2C between the two servers. In contrast to existing approaches, which only approximate the activation functions by polynomials, our approach preserves the accuracy.

<div style="text-align:center">

TABLE 2
Notations

</div>

C	$(m \times m)$ convolutional kernels of CNN
$f(x)$	non-polynomial activation function
$\mathcal{G}$	original image (of pixel size $n \times n$)
$\mathcal{H}$	convoluted image
$\mathcal{J}$	activated image
$q \times q$	size of the pooling window
$\mathcal{K}$	down-sampled image
W	weight matrix in fully-connected layer
$\mathcal{F}$	prediction results
$\cdot$	inner product operation

- We also replace the non-polynomial max-pooling function with the average-pooling function, which is a linear function for further efficiency improvement. In our experiment, we train with the MNIST dataset and CIFAR dataset. Our results demonstrate that the final accuracy of average-pooling is comparable to that of max-pooling.
- Our experiments on MNIST dataset show that our scheme achieves $122\times$, $14.63\times$, and $8.19\times$ lower latency than SecureML [40], MiniONN [23], and EzPC [27], respectively. For the communication costs, our scheme outperforms SecureML by $1.09\times$, MiniONN by $36.69\times$, and EzPC by $31.32\times$. Our scheme also incurs $7.14\times$ and $3.48\times$ lower computation costs, and $13.88\times$ and $77.46\times$ lower communication costs, than MiniONN and EzPC on the CIFAR dataset.
- We provide a security analysis in the simulation paradigm to show the privacy of our scheme.

2 PRELIMINARY

2.1 Convolutional Neural Network (CNN) and Notations

We use image processing as a running example since CNN is good at such kind of tasks. A typical CNN consists of four classes of layers. The core one is the *convolutional layer*. It computes the convolution, essentially an *inner product*, between the raw pixel values in each local region of the image and a set of the convolutional kernel. Table 2 lists our major notation. For the inner product (denoted by $\cdot$) of two matrices, we first transform the matrices into vectors.

Let $\mathcal{G}$ be the query image as an $n \times n$ matrix of 8-bit pixel. For simplicity, we consider only one convolution kernel C each of size $m \times m$ (*i.e.*, the padding mode is ''same''). The convolution transforms $\mathcal{G}$ into a matrix $\mathcal{H}$.

After the convolutional layer, it is usually the *activation layer*, which applies an element-wise *non-polynomial* activation function for increasing the nonlinear properties of the model. We use the most fashionable ReLU function, which only keeps the positive part of any real-valued input (*i.e.*, $f(x) = \max(0, x)$). We let $\mathcal{J}$ be the image activated by $f(x)$, which remains of size $n \times n$.

The *pooling layer* performs a down-sampling along the spatial dimensions while retaining critical information. The usual ones are *max-pooling* and *average-pooling*, which

outputs the maximum or the average value of the pool. The size of the pool is $q \times q$. The resulting smaller image $\mathcal{K}$ is of size $(n/q)^2$.

The final layer is the *fully-connected layer*. The image matrix in the previous layer is first transformed into a column vector of dimension being the neuron numbers of the first layer in the fully-connected layer, *i.e.*, each element in the vector is the input of the corresponding neuron. Every neuron in the previous layer is connected to every neuron in the next layer. The weight matrix of the fully-connected layer is denoted by W. By the scalar product of the output of the previous layer and the corresponding weight matrix, we obtain a column vector, each of its elements corresponds to the input of the next layer. The output of the last layer is deemed as the final prediction results.

The classes with the desired scores form the final prediction result $\mathcal{F}$, which correspond to the most probable category. Our goal is to let the querier learn $\mathcal{F}$ without revealing the query $\mathcal{G}$ and the neural network to the servers.

2.2 Cryptographic Tools

2.2.1 Secure Two-Party Computation (S2C)

S2C allows two parties to jointly compute a function over their private inputs while warranting the correctness. No party learns anything about the other's input beyond what is implied by the function. *Garbled circuits* proposed by Yao [43] can evaluate arbitrary function represented as a boolean circuit. During the evaluation, no party learns anything about the input data of others beyond what is implied by the final results.

2.2.2 Secret Sharing

Many S2C protocols [45] operate on secret-shared inputs. Secret sharing allows one to distribute a secret by distributing shares to each of many parties. In (t, n)-Shamir secret sharing [41], there are n shares, which are random elements of a finite field. Any set of at least t shares allows recovery of the secret value via Lagrange interpolation of a degree $(t - 1)$ polynomial embedding the secret. Any non-qualifying set of shares looks randomly distributed, which provides perfect confidentiality.

In this paper, we use $(2, 2)$-secret sharing or simply additive secret sharing, in which the two shares add up to the secret value in the field. Specifically, consider the secret to be shared is s, which is encoded as a t-bit string. One can pick a t-bit string r uniformly at random. The shares are r and $s - r \mod 2^t$. For sure, r alone is random, and $s - r \mod 2^t$ alone is random too since, for every candidate s', one must be able to find the corresponding r' such that $s' - r' = s - r$ due to the existence of the additive inverse.

We operate on the secret-shared values extensively. We use a unified notation of superscript 1 or 2 to denote the shared information of servers $\mathcal{S}_1$ or $\mathcal{S}_2$. For examples, the shared image held by $\mathcal{S}_1$ and $\mathcal{S}_2$ are $\mathcal{G}^1$ and $\mathcal{G}^2$ respectively, and the i-th row and j-th column entry held by $\mathcal{S}_1$ are $\mathcal{G}^1_{i,j}$.

① Secret-Sharing Query   ② Convolution   ③ Activation   ④ Pooling   ⑤ Fully connected   ⑥ Prediction
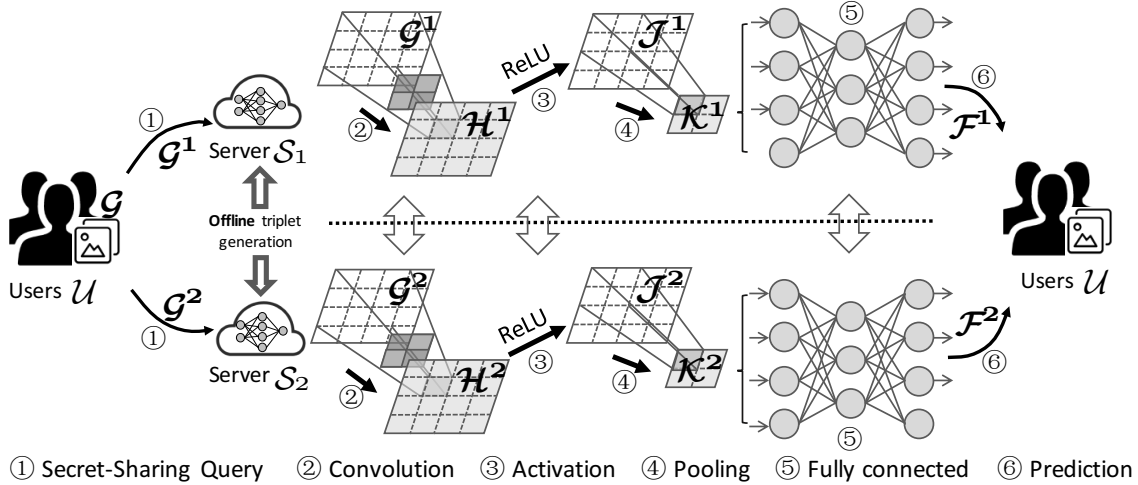
Fig. 1. An overview of our scheme: ReLU means rectified linear unit, which is an activation function. The notations $\mathcal{G}, \mathcal{H}, \mathcal{J}, \mathcal{K}, \mathcal{F}$ are described in Table 2. The superscript 1 or 2 denotes the secret-shared information belong to $\mathcal{S}_1$ or $\mathcal{S}_2$.

2.2.3 Homomorphic Encryption (HE)

HE (*e.g.*, [28], [46]) allows computations over encrypted data without access to the secret key. Decrypting the resultant ciphertexts gives the computation result of the operations as if they had been performed on the plaintext. For the public/private key pair (pk, sk), and an encryption of x denoted by $[\![x]\!]_{pk}$, we have homomorphisms $\oplus$ and $\otimes$ where $[\![a]\!]_{pk} \oplus [\![b]\!]_{pk} = [\![a + b]\!]_{pk}$, $[\![a]\!]_{pk} \otimes [\![b]\!]_{pk} = [\![a \times b]\!]_{pk}$. Following MiniONN [23], this work uses the ring-based FHE scheme called YASHE [46]. It offers a plaintext space that is large enough for usual computation. With SIMD [44], 4096 independent plaintexts in our application can be packed to one ciphertext and operated in parallel, which reduces the communication and computation.

3 OUR CONSTRUCTION

3.1 System Model and Threat Model

Fig. 1 illustrates our system model. In an initialization stage, the model owner (not depicted) secret-shares the model (including the convolutional kernel and the weight in the fully-connected layer) between two servers, $\mathcal{S}_1$ and $\mathcal{S}_2$. One of them also needs to set up a public/private key pair, to be described in Section 3.3.1. Such public key is just for accelerating the triplet generation in an offline preparation stage, but not used in the online computation. Section 3.2 discusses the triplet generation in detail.

To use the prediction service, user $\mathcal{U}$ secret-shares the query into two shares and send them to $\mathcal{S}_1$ and $\mathcal{S}_2$, respectively, to be described in Section 3.3.2. $\mathcal{S}_1$ interacts with $\mathcal{S}_2$ to make predictions based on the secret shares.

For each stage of the online prediction (including convolution computation, activation computation, pooling computation, fully-connected layer), we design secure interactive protocols to achieve effective computation. Our protocols rely on the fact that the input (output) of each stage is secret-shared between two servers, and thus the sum of computation results from the two shares is equal to the computation result from the original input. Section 3.3.3 to Section 3.3.6 discuss the computation of each layer. To further reduce the online overheads, we design the accelerated asynchronous online computations as presented in Section 3.4. After interactions, the servers derive and return their corresponding shared results to $\mathcal{U}$, who can then recover the real prediction result locally.

We assume that $\mathcal{S}_1$ and $\mathcal{S}_2$ are honest-but-curious and do not collude with each other. Most service providers are motivated to maintain their reputation instead of risking it with collusion. With this assumption, our goal becomes ensuring both $\mathcal{S}_1$ and $\mathcal{S}_2$ cannot learn any information about the model, the query from $\mathcal{U}$, and the (intermediate) prediction results. Intuitively, this gives us hope for higher efficiency without greatly affecting accuracy.

3.2 Accelerated Triplet Generation

The convolutional and fully-connected layers involve many inner-product computations. To reduce the cost of online computation over secret shares. $\mathcal{S}_1$ and $\mathcal{S}_2$ first prepare the multiplicative triplets [42]. Specifically, $\mathcal{S}_1$ holds a_1 and b_1, $\mathcal{S}_2$ holds a_2 and b_2. They want to compute the multiplication of $a = a_1 + a_2$ and $b = b_1 + b_2$ in a shared form *i.e.*, $\mathcal{S}_1$ obtains z_1, $\mathcal{S}_2$ obtains z_2 where $z_1 + z_2 = ab$. Fig. 2 presents the triplets generation algorithm TRIP. We have $ab = (a_1 + a_2)(b_1 + b_2) = a_1 b_1 + a_1 b_2 + a_2 b_1 + a_2 b_2$. It is easy for $\mathcal{S}_1$ and $\mathcal{S}_2$ to locally compute $a_1 b_1$ and $a_2 b_2$, respectively.

To compute $a_1 b_2$ and $a_2 b_1$, $\mathcal{S}_1$ first encrypts a_1 and b_1 and sends the ciphertexts to $\mathcal{S}_2$. So, $\mathcal{S}_2$ can add V_1, V_2, which are HE encryption of $a_1 b_2$ and $a_2 b_1$ respectively, and a random number r together to obtain V_3 via additive homomorphism, without any information leakage. The shared result of $\mathcal{S}_2$ is $z_2 = a_2 b_2 - r$. By decrypting V_3, $\mathcal{S}_1$ obtains v, which is added to $a_1 b_1$ to obtain the shared result $z_1 = ab - a_2 b_2 + r$. In this way, the shared results z_1 and z_2 can recover the multiplication result z by simple addition, but neither $\mathcal{S}_1$ nor $\mathcal{S}_2$ can learn z. This preparation is done in an offline phase.

The triplet generation involves many homomorphic operations. To further speed up the triplet generation process, we adopt data packing and asynchronous computation.

$$\text{tri} \leftarrow \text{TRIP}(a_1, b_1, (pk, sk); a_2, b_2, pk)$$

Require: $\mathcal{S}_1$ holds $a_1, b_1 \in \mathbb{Z}_{2^t}$ and the key pair (pk, sk). $\mathcal{S}_2$ holds the other shares $a_2 = (a - a_1) \bmod 2^t$, $b_2 = (b - b_1) \bmod 2^t$ and the public key pk.

Ensure: $\mathcal{S}_1$ gets $\text{tri}^1 = (a_1, b_1, z_1)$. $\mathcal{S}_2$ gets $\text{tri}^2 = (a_2, b_2, z_2)$, where $z = z_1 + z_2 = a \cdot b \bmod 2^t$.

At $\mathcal{S}_1$ side:
  1) Encrypt a_1 and b_1 to have $[\![a_1]\!]_{pk}$ and $[\![b_1]\!]_{pk}$;
  2) Send the ciphertexts $[\![a_1]\!]_{pk}$ and $[\![b_1]\!]_{pk}$ to $\mathcal{S}_2$.

At $\mathcal{S}_2$ side:
  1) Compute $V_1 = [\![a_1 \cdot b_2]\!]_{pk} = [\![a_1]\!]_{pk} \otimes [\![b_2]\!]_{pk}$,
    $V_2 = [\![a_2 \cdot b_1]\!]_{pk} = [\![b_1]\!]_{pk} \otimes [\![b_1]\!]_{pk}$;
  2) Send $V_3 = V_1 \oplus V_2 \oplus [\![r]\!]_{pk}$ to $\mathcal{S}_1$, where $r \in \mathbb{Z}_{2^t}$;
  3) Set $z_2 = (a_2 \cdot b_2 - r) \bmod 2^t$.

At $\mathcal{S}_1$ side:
  1) Decrypt V_3 to have $v = a_1 \cdot b_2 + a_2 \cdot b_1 + r$;
  2) Set $z_1 = (v + a_1 \cdot b_1) = (a \cdot b - a_2 \cdot b_2 + r) \bmod 2^t$.

The triplet is $\text{tri} = ((a_1, a_2), (b_1, b_2), (z_1, z_2))$.

Fig. 2. Secure triplet generation protocol TRIP

3.2.1 Data Packing

Considering n shares $\langle a_1^i, b_1^i, a_2^i, b_2^i \rangle_{i=1}^n$, we pack $\langle a_1^i \rangle_{i=1}^n$ together to be a single plaintext A_1 to generate n triplets simultaneously. Analogously, we compute the packed data $B_1 = \langle b_1^i \rangle_{i=1}^n$, $A_2 = \langle a_2^i \rangle_{i=1}^n$, and $B_2 = \langle b_2^i \rangle_{i=1}^n$. The homomorphic operations are then performed on the packed data via SIMD [44] to get the packed triplets $((A_1, A_2), (B_1, B_2), (Z_1, Z_2))$. They can then be unpacked to extract the real triplets $\langle (a_1^i, a_2^i), (b_1^i, b_2^i), (z_1^i, z_2^i) \rangle_{i=1}^n$, where $z_1^i + z_2^i = (a_1^i + a_2^i) \cdot (b_1^i + b_2^i)$. In essence, our approach reduces the encryption, transmission, addition, and multiplication costs. We refer to Appendix A for a toy example for the packed triplet generation process.

3.2.2 Asynchronous Computation

$\mathcal{S}_1$ and $\mathcal{S}_2$ have to wait for the intermediate results from the other while generating the triplets. We call this synchronous computation. To speed it up, we design an asynchronous computation scheme. Instead of waiting for the feedback, the servers continue the remaining operations that do not involve the feedback. For example, $\mathcal{S}_1$ can encrypt b_1 when transforming the ciphertext a_1. $\mathcal{S}_2$ can encrypt the random number r and compute $a_2 b_2$ ahead of time. Such asynchronous computation reduces the waiting time and the latency. See Appendix A for an illustration.

3.3 Our Scheme

3.3.1 Initialization

$\mathcal{S}_1$ possesses one share of the prediction model, *i.e.*, the convolutional kernel C^1 and the weight matrix W^1, and the HE key pair (pk, sk). $\mathcal{S}_2$ owns the other share of the prediction model (*i.e.*, C^2 and W^2) and the public key pk. $\mathcal{U}$ holds the query image $\mathcal{G}$. They then engage in the TRIP protocol to generate enough number of multiplicative triplets $\text{tri} = ((A_1, A_2), (B_1, B_2), (Z_1, Z_2))$.

$$(\mathcal{H}^1; \mathcal{H}^2) \leftarrow \text{CONV}(\mathcal{G}^1, \mathsf{C}^1, (pk, sk); \mathcal{G}^2, \mathsf{C}^2, pk)$$

Require: $\mathcal{S}_1$ holds the shares of image $\mathcal{G}^1$, the convolutional kernel C^1, and the shared triplet $(A_1 = \langle a_1^k \rangle, B_1 = \langle b_1^k \rangle, Z_1 = \langle z_1^k \rangle)$; $\mathcal{S}_2$ holds shares $\mathcal{G}^2$, C^2, and shared triplet $(A_2 = \langle a_2^k \rangle, B_2 = \langle b_2^k \rangle, Z_2 = \langle z_2^k \rangle)$. We have $z_1^k + z_2^k = (a_1^k + a_2^k)(b_1^k + b_2^k)$ or $Z_1 + Z_2 = AB$.

Ensure: $\mathcal{S}_1, \mathcal{S}_2$ get shared convoluted images $\mathcal{H}^1, \mathcal{H}^2$ respectively, where $\mathcal{H}^1 + \mathcal{H}^2 = (\mathcal{G}^1 + \mathcal{G}^2) \cdot (\mathsf{C}^1 + \mathsf{C}^2)$.

$\mathcal{S}_1$ and $\mathcal{S}_2$:
  1) **for** i, j **in** range n
  - Choose the sub-image $\langle \mathcal{G}_{p,q}^1 \rangle_{p,q=i-\frac{m-1}{1}}^{p,q=i+\frac{m-1}{1}}$ as vector $\tilde{\mathcal{G}}_{i,j}^1$ and $\langle \mathcal{G}_{p,q}^2 \rangle_{p,q=i-\frac{m-1}{1}}^{p,q=i+\frac{m-1}{1}}$ as vector $\tilde{\mathcal{G}}_{i,j}^2$;
  - $\mathcal{S}_1$ sends $U^1 = \tilde{\mathcal{G}}_{i,j}^1 - A_1, V^1 = \mathsf{C}^1 - B_1$ to $\mathcal{S}_2$,
    $\mathcal{S}_2$ sends $U^2 = \tilde{\mathcal{G}}_{i,j}^2 - A_2, V^2 = \mathsf{C}^2 - B_2$ to $\mathcal{S}_1$;
  - $\mathcal{S}_1$ and $\mathcal{S}_2$ compute $U = \tilde{\mathcal{G}}_{i,j} - A, V = \mathsf{C} - B$;
  - $\mathcal{S}_1$ computes $\mathcal{H}_{i,j}^1 = -UV + \tilde{\mathcal{G}}_{i,j}^1 V + \mathsf{C}^1 U + Z_1$,
    $\mathcal{S}_2$ computes $\mathcal{H}_{i,j}^2 = \tilde{\mathcal{G}}_{i,j}^2 V + \mathsf{C}^2 U + Z_2$.
  2) Return $\mathcal{H}^1$ and $\mathcal{H}^2$.

Fig. 3. Secure convolution computation protocol CONV

3.3.2 Secret-Sharing the Query

$\mathcal{U}$ randomly secret-shares the pixel $\mathcal{G}_{i,j}$ ($i, j \in [1, n]$) of query $\mathcal{G}$ into $\mathcal{G}_{i,j}^1$ and $\mathcal{G}_{i,j}^2$ as $\mathcal{G}_{i,j} = \mathcal{G}_{i,j}^1 + \mathcal{G}_{i,j}^2 \bmod 2^t$, where $\mathcal{G}_{i,j}^1$ is chosen from $[0, 2^t - 1]$ uniformly at random. $\mathcal{G}^1$ and $\mathcal{G}^2$ are distributed to $\mathcal{S}_1$ and $\mathcal{S}_2$, respectively. From the perspective of the server, the received query, either as $\mathcal{G}^1$ or $\mathcal{G}^2$, is random by itself.

3.3.3 Convolution Computation

Fig. 3 describes our secure convolution computation protocol (CONV). Given the secret-shared query ($\mathcal{G}^1$, $\mathcal{G}^2$) and the secret-shared convolutional kernel (C^1, C^2) as input, the two servers run the CONV protocol and output the shared results $\mathcal{H}^1$ and $\mathcal{H}^2$ such that $\mathcal{H}^1 + \mathcal{H}^2 = \mathcal{G} \cdot \mathsf{C}$.

In more detail, $\mathcal{S}_1$ and $\mathcal{S}_2$ apply convolution over each sub-image $\tilde{\mathcal{G}}_{i,j}^1$ and $\tilde{\mathcal{G}}_{i,j}^2$ of the size $m \times m$ from the shared images $\mathcal{G}^1$ and $\mathcal{G}^2$, respectively. With tri prepared by the execution of TRIP in the offline phase, $\mathcal{S}_1$ ($\mathcal{S}_2$) uses A_1 (A_2) as a one-time pad to hide the sub-images $\tilde{\mathcal{G}}_{i,j}^1$ (resp. $\tilde{\mathcal{G}}_{i,j}^2$)). Likewise, they use B_1 (B_2) to hide the convolutional kernel C^1 (resp. C^2). After they exchanged these padded shares, they can locally compute $\mathcal{H}^1$ and $\mathcal{H}^2$. For correctness:

$$
\begin{aligned}
&\mathcal{H}^1 + \mathcal{H}^2 \\
={}& (-UV + \tilde{\mathcal{G}}_{i,j}^1 V + \mathsf{C}^1 U + Z_1) + (\tilde{\mathcal{G}}_{i,j}^2 V + \mathsf{C}^2 U + Z_2) \\
={}& -UV + (\tilde{\mathcal{G}}_{i,j}^1 V + \tilde{\mathcal{G}}_{i,j}^2 V) + (\mathsf{C}^1 U + \mathsf{C}^2 U) + (Z_1 + Z_2) \\
={}& -(\tilde{\mathcal{G}}_{i,j} - A)V + \tilde{\mathcal{G}}_{i,j} V + \mathsf{C} U + AB \\
={}& AV + \mathsf{C} U + AB \\
={}& A(\mathsf{C} - B) + \mathsf{C}(\tilde{\mathcal{G}}_{i,j} - A) + AB \\
={}& \tilde{\mathcal{G}}_{i,j} \cdot \mathsf{C}.
\end{aligned}
$$
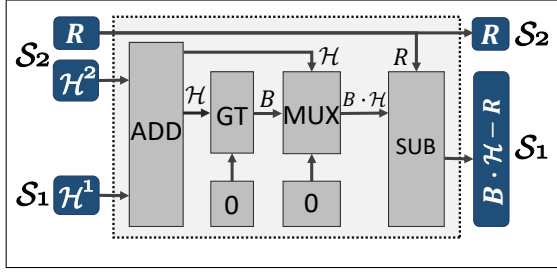
Fig. 4. Our (garbled) circuits for ReLU activation function ActF

3.3.4 Activation Computation

$\mathcal{S}_1$ and $\mathcal{S}_2$ use the garbled circuit ActF in Fig. 4 to compute the activation function over $\mathcal{H}^1$ and $\mathcal{H}^2$. The circuit utilizes four sub-circuits:

- ADD(a, b) outputs the sum $a + b$;
- GT(a, b) returns the bit denoting if $a > b$;
- MUX(a, b, c) outputs a or b according to c, i.e., if c holds, MUX$(a, b, c) = b$, otherwise MUX$(a, b, c) = a$; and
- SUB(a, b) returns the difference $a - b$.

$\mathcal{S}_1$ and $\mathcal{S}_2$ run ActF with $\mathcal{H}^1$ and $(\mathcal{H}^2, R)$ being the respective inputs, where R is a random matrix generated by $\mathcal{S}_2$. The outputs of $\mathcal{S}_1$ and $\mathcal{S}_2$ are $(0|1) \cdot \mathcal{H} - R$ and R, respectively, where $(0|1)$ denotes a variable of value either 0 or 1 depending on $\mathcal{H}$. To summarize in the standard S2C notation, $((0|1) \cdot \mathcal{H} - R; R) \leftarrow \mathsf{ActF}(\mathcal{H}^1; (\mathcal{H}^2, R))$.

Specifically, ADD$(\mathcal{H}^1, \mathcal{H}^2)$ adds $\mathcal{H}^1$ and $\mathcal{H}^2$ to get $\mathcal{H}$. Then, GT$(\mathcal{H}, 0)$ compares $\mathcal{H}$ and 0 element-wise for ReLU. The output is a binary matrix B of the same size as $\mathcal{H}$, where the pixel $B_{i,j} = 1$ if $\mathcal{H}_{i,j} > 0$, 0 otherwise. With B, MUL$(\mathcal{H}, 0, B)$ performs activation function, i.e., if $\mathcal{H}_{i,j} > 0$ ($B_{i,j} = 1$), outputs $\mathcal{H}$, otherwise outputs 0. Finally, SUB makes element-wise subtraction to have $B \cdot \mathcal{H} - R$, which is the output of $\mathcal{S}_1$. Let $\mathcal{J}$ be the activated image $B \cdot \mathcal{H}$. $\mathcal{J}^1 = B \cdot \mathcal{H} - R$. The output of $\mathcal{S}_2$ is regarded as $\mathcal{J}^2 = R$.

3.3.5 Pooling Computation

Fig. 5 shows the POOL "protocol" for element-wise average-pooling over $(\mathcal{J}^1, \mathcal{J}^2)$ to obtain $(\mathcal{K}^1, \mathcal{K}^2)$. $\mathcal{S}_1$ and $\mathcal{S}_2$ run POOL with the activated shared data $\mathcal{J}^1$ and $\mathcal{J}^2$ being the respective inputs. The outputs of $\mathcal{S}_1$ and $\mathcal{S}_2$ are the secret-shared pooled results $\mathcal{K}^1$ and $\mathcal{K}^2$, respectively.

The pixel value $\mathcal{K}_{i,j}^1$ is the average of the corresponding $q \times q$ pixels in $\mathcal{J}^1$. Analogously, $\mathcal{K}_{i,j}^2$ can be derived from $\mathcal{J}^2$. Employing the average value to replace the original pixels, we can reduce $\mathcal{J}$ to the down-sampled image $\mathcal{K}$ of size $\lceil \frac{n}{q} \rceil \times \lceil \frac{n}{q} \rceil$.

$$(\mathcal{J}_1^1 + \mathcal{J}_2^1 + \cdots + \mathcal{J}_{q^2}^1)/q^2 + (\mathcal{J}_1^2 + \mathcal{J}_2^2 + \cdots + \mathcal{J}_{q^2}^2)/q^2$$
$$= (\mathcal{J}_1 + \mathcal{J}_2 + \cdots + \mathcal{J}_{q^2})/q^2.$$

It is easy to see that they can perform the above computation locally without any interaction.

3.3.6 Fully-Connected-Layer Computation

Finally, the fully-connected layer, in essence, performs dot products between the pooled data $\mathcal{K}$ and the weight parameters W, which can be computed using the triplets similar to that in the convolutional layer illustrated in

$(\mathcal{K}^1; \mathcal{K}^2) \leftarrow \mathsf{POOL}(\mathcal{J}^1; \mathcal{J}^2)$

Require: $\mathcal{S}_1$ holds the shared activated image $\mathcal{J}_1$; $\mathcal{S}_2$ holds the other shares $\mathcal{J}_2$.
Ensure: $\mathcal{S}_1$ obtains the shared pooled image $\mathcal{K}_1$; $\mathcal{S}_2$ holds the other share $\mathcal{K}_2$. $\mathcal{K}_1 + \mathcal{K}_2 = pooling(\mathcal{J}_1 + \mathcal{J}_2)$.
At $\mathcal{S}_1$ side:
  1) **for** i, j **in** range $\lfloor \frac{n}{q} \rfloor$
    - Compute $\frac{1}{q \times q} \sum_{u=0}^{u=q-1} \sum_{v=0}^{v=q-1} \mathcal{J}_{qi-u, qj-v}^1$.
    - Set the averages as the value of $\mathcal{K}_{i,j}^1$.
At $\mathcal{S}_2$ side:
  1) **for** i, j **in** range $\lfloor \frac{n}{q} \rfloor$
    - Compute $\frac{1}{q \times q} \sum_{u=0}^{u=q-1} \sum_{v=0}^{v=q-1} \mathcal{J}_{qi-u, qj-v}^2$.
    - Set the averages as the value of $\mathcal{K}_{i,j}^2$.

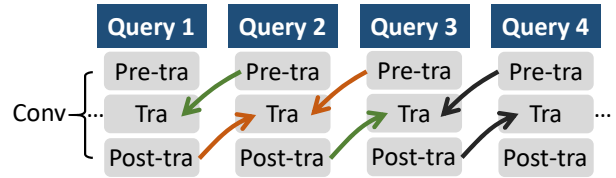Fig. 5. Secure pooling computation protocol

Fig. 6. Asynchronous computation for online prediction

Fig. 3. We skip the largely repetitive details. Specifically, $\mathcal{S}_1$ and $\mathcal{S}_2$ take as input the shares $\mathcal{K}^1, W^1$ and $\mathcal{K}^2, W^2$ respectively, resulting in the shared prediction results $\mathcal{F}^1$ and $\mathcal{F}^2$. User $\mathcal{U}$ can merge $\mathcal{F}^1$ and $\mathcal{F}^2$ to recover the prediction result $\mathcal{F} = \mathcal{K}W$.

3.4 Accelerated Asynchronous Online Computations

Finally, we remark that we can accelerate convolution and fully-connected layers by simultaneously conducting computations (of U^1, V^1, U^2, V^2 (pre-transmission), $U, V, \mathcal{H}_{i,j}^1, \mathcal{H}_{i,j}^2$ (post-transmission)) and transmission (of U^1, V^1, U^2, V^2). Fig. 6 depicts asynchronous computations in the convolution layers. The computation process at the tail of the arrow is in parallel with the transmission process at the arrowhead. For example, the pre-transmission and post-transmission operations of query 2 are in parallel with the transmission of query 1 and query 3, respectively.

4 PERFORMANCE EVALUATION

4.1 Experimental Setup and Dataset

Our experiments use separate machines for $\mathcal{U}$, $\mathcal{S}_1$, and $\mathcal{S}_2$. Each has an Intel 4-Core CPU operating at 1.60 GHz with 8 GB RAM, running Ubuntu 18.04 as the operating system. We implemented our scheme in C++ with Python binding. For garbled circuits, we use the ABY library with SIMD circuits [45]. Following MiniONN, we use YASHE for FHE and implement it by the SEAL library [47], supporting SIMD. In YASHE, the degree of the polynomial n is set to be 4096. In this way, we can pack 4096 elements together. The plaintext modulus is $101,285,036,033$. The length of the plaintext is 64-bit. The ciphertext modulus is 128-bit.

1) *Convolution*: input image 28×28, window size 5×5, stride$(1, 1)$, number of output channels of 16: $\mathbb{R}^{16 \times 576} \leftarrow \mathbb{R}^{16 \times 25} \times \mathbb{R}^{25 \times 576}$.
2) *ReLU Activation*: calculates ReLU for each input.
3) *Average Pooling*: window size $1 \times 2 \times 2$ and outputs $\mathbb{R}^{16 \times 12 \times 12}$.
4) *Convolution*: input image 12×12, window size 5×5, stride $(1, 1)$, number of output channels of 16: $\mathbb{R}^{16 \times 64} \leftarrow \mathbb{R}^{16 \times 400} \times \mathbb{R}^{400 \times 64}$.
5) *ReLU Activation*: calculates ReLU for each input.
6) *Average Pooling*: window size $1 \times 2 \times 2$ and outputs $\mathbb{R}^{16 \times 4 \times 4}$.
7) *Fully Connected*: fully connects the incoming 256 notes to the outgoing 100 nodes: $\mathbb{R}^{100 \times 1} \leftarrow \mathbb{R}^{100 \times 256} \times \mathbb{R}^{256 \times 1}$.
8) *ReLU Activation*: calculates ReLU for each input.
9) *Fully Connected*: fully connects the incoming 100 notes to the outgoing 10 nodes: $\mathbb{R}^{10 \times 1} \leftarrow \mathbb{R}^{10 \times 100} \times \mathbb{R}^{100 \times 1}$.

Fig. 7. The neural network architecture on MNIST dataset

These parameters matter in Section 4.3. All results are averaged over at least 5 runs, in which the error is controlled within 3%.

We conduct experiments over two standard datasets, MNIST [48] and CIFAR-10 [49]. The MNIST dataset [48] consists of $60,000$ grayscale images of hand-written digit belong to 10 classes, each 28×28 pixels. The CIFAR-10 dataset [49] contains $60,000$ color images of size 32×32 pixels in 10 different classes.

Apart from real datasets, a realistic neural network model is also important to demonstrate our system performance. Fig. 7 and Fig. 8 detail the neural network architectures we used (following MiniONN [23]) on MNIST and CIFAR-10 dataset, respectively.

4.2 Accuracy Evaluation

4.2.1 Effect of Pooling Method

To evaluate the effect of average-pooling and max-pooling, we trained the model on the MNIST and CIFAR-10 datasets for each pooling method. Fig. 9 and Fig. 10 plot the accuracy against the training epoch for the MNIST and CIFAR datasets, respectively. The light blue line represents the accuracy using max-pooling, and the dark blue line shows the accuracy using average-pooling.

The accuracy grows with the epochs until stabilized. For the MNIST dataset, after 10 epochs, the accuracy of max-pooling reaches 98.7%, while that of average-pooling is just 98.2%. After 100 epochs, the accuracy of max-pooling achieves 99.1%, and that of average-pooling achieves 99.0%, with a difference of 0.1%. For the CIFAR-10 dataset, after 10 epochs, max-pooling achieves an accuracy of 72% while average-pooling achieves an accuracy of 65%. After 100 epochs, the accuracy of max-pooling is 74%, and that of average-pooling is 73%, with a difference of 1% again. To conclude, their accuracy differs by just 1%, which is acceptable in most application scenarios. That said, we remark that it could be too big in life-critical applications such as disease diagnosis.

1) *Convolution*: input image 32×32, window size 3×3, stride$(1, 1)$, number of output channels of 64: $\mathbb{R}^{64 \times 1024} \leftarrow \mathbb{R}^{64 \times 27} \times \mathbb{R}^{27 \times 1024}$.
2) *ReLU Activation*: calculates ReLU for each input.
3) *Convolution*: window size 3×3, stride$(1, 1)$, number of output channels of 64: $\mathbb{R}^{64 \times 1024} \leftarrow \mathbb{R}^{64 \times 576} \times \mathbb{R}^{576 \times 1024}$.
4) *ReLU Activation*: calculates ReLU for each input.
5) *Average Pooling*: window size $1 \times 2 \times 2$ and outputs $\mathbb{R}^{64 \times 16 \times 16}$.
6) *Convolution*: window size 3×3, stride $(1, 1)$, number of output channels of 64: $\mathbb{R}^{64 \times 256} \leftarrow \mathbb{R}^{64 \times 576} \times \mathbb{R}^{576 \times 256}$.
7) *ReLU Activation*: calculates ReLU for each input.
8) *Convolution*: window size 3×3, stride $(1, 1)$, number of output channels of 64: $\mathbb{R}^{64 \times 256} \leftarrow \mathbb{R}^{64 \times 576} \times \mathbb{R}^{576 \times 256}$.
9) *ReLU Activation*: calculates ReLU for each input.
10) *Average Pooling*: window size $1 \times 2 \times 2$ and outputs $\mathbb{R}^{64 \times 8 \times 8}$.
11) *Convolution*: window size 3×3, stride $(1, 1)$, number of output channels of 64: $\mathbb{R}^{64 \times 64} \leftarrow \mathbb{R}^{64 \times 576} \times \mathbb{R}^{576 \times 64}$.
12) *ReLU Activation*: calculates ReLU for each input.
13) *Convolution*: window size 1×1, stride $(1, 1)$, number of output channels of 64: $\mathbb{R}^{64 \times 64} \leftarrow \mathbb{R}^{64 \times 64} \times \mathbb{R}^{64 \times 64}$.
14) *ReLU Activation*: calculates ReLU for each input.
15) *Convolution*: window size 1×1, stride $(1, 1)$, number of output channels of 64: $\mathbb{R}^{16 \times 64} \leftarrow \mathbb{R}^{16 \times 64} \times \mathbb{R}^{64 \times 64}$.
16) *ReLU Activation*: calculates ReLU for each input.
17) *Fully Connected*: fully connects the incoming 1024 notes to the outgoing 10 nodes: $\mathbb{R}^{10 \times 1} \leftarrow \mathbb{R}^{10 \times 1024} \times \mathbb{R}^{1024 \times 1}$.

Fig. 8. The neural network architecture on the CIFAR-10 dataset

4.2.2 Effect of Activation Function

Some FHE-based schemes [21], [33] approximate the activation function by polynomials. Fig. 11 plots the curves of the original ReLU function and its approximations with different degrees, which are polynomial regression function *polyfit* from the Python package `numpy`.

The approximation is satisfactory when the absolute value of the input is smaller than 4. However, for larger input, the error introduced by the approximation becomes very large, which in turn affects the prediction accuracy. Our scheme reaches the same accuracy as plaintext computation by directly designing the garbled circuits for ReLU, which compute an identical output as ReLU.

4.3 Efficiency Evaluation

4.3.1 Triplet Generation

Table 3 compares our triplets generation method with prior work in terms of the computational complexity. As Fig. 2, triplet generation for two n-dimensional shared vectors of SecureML [40] encrypts each element of the shared vector, respectively. This process consists of $5n$ Enc encryptions,
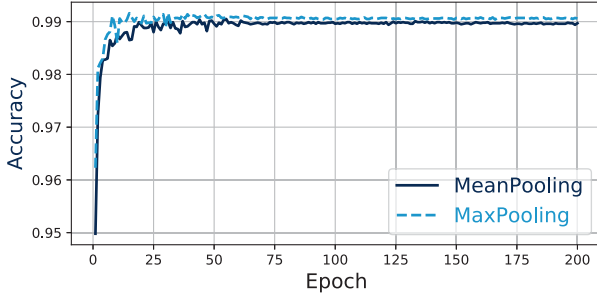
Fig. 9. Accuracy of the trained model with different pooling methods on MNIST dataset
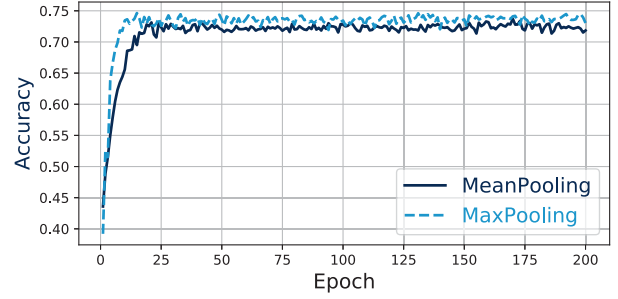

Fig. 10. Accuracy of the trained model with different pooling methods on CIFAR-10 dataset
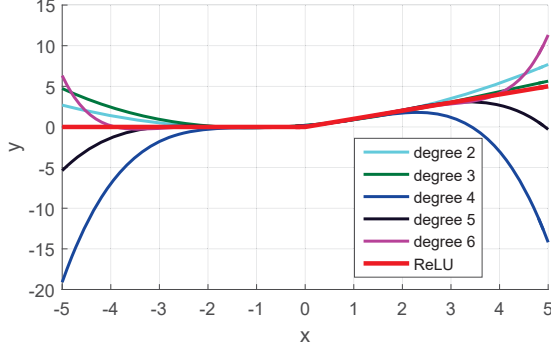

Fig. 11. Approximate function of ReLU activation function

TABLE 4
Triplet generation costs (ms)

Original triplet generation	Packed triplet generation	Packed triplet generation with Asyn. Comp.	Performance Gain
79716.524	19.635	16.970	4697×

TABLE 5
ReLU costs (ms)

	Offline	Online	Avg. Offline	Avg. Online
$\mathcal{S}_1$	87.815	752.545	0.021	0.184
$\mathcal{S}_2$	100.143	516.413	0.024	0.126

TABLE 3
Comparison of triplet generation

Methodology	Complexity	Required operations
SecureML [40]	$\mathcal{O}(n)$	n·(5Enc + 2CMul + 2Add + 1Dec)
MiniONN [23]	$\mathcal{O}(n/l)$	$\frac{n}{l}$·(5Enc + 2CMul + 2Add + 1Dec)
Our Scheme	$\mathcal{O}(n/l)$	$\frac{n}{l}$·(5Enc + 2CMul + 2Add + 1Dec)

Enc: encryption; CMul: constant multiplication over ciphertext; Add: addition between two ciphertexts; Dec: decryption

TABLE 6
Polynomial approximation

Approximate Function	Time (ms)	Performance Gain
$0.1992 + 0.5002x + 0.1997x^2$	19.02	61×
$0.1995 + 0.5002x + 0.1994x^2 - 0.0164x^3$	38.00	123×
$0.1500 + 0.5012x + 0.2981x^2 - 0.0004x^3 - 0.0388x^4$	69.62	225×
$0.1488 + 0.4993x + 0.3007x^2 + 0.0003x^3 - 0.0168x^4$	69.64	224×
$0.1249 + 0.5000x + 0.3729x^2 - 0.0410x^4 + 0.0016x^6$	82.20	265×

$2n$ CMul multiplications and additions, n decryptions, in which n ciphertexts are transferred between the two servers.

In contrast, MiniONN [23] and our scheme use the packing technique. All the l elements can be computed at the same time. The n-dimensional vector is compressed into an (n/l)-dimensional vector. This means that the complexity of MiniONN and our scheme is just $\mathcal{O}(n/l)$.

Table 4 shows that our packed triplet generation is several order-of-magnitude faster. Further adopting asynchronous computations improves the efficiency by 13.6%, resulting in an overall speedup of $4697\times$.

4.3.2 Activation Function

To make our contribution stand out, we run the activation function circuits alone to demonstrate its performance. Table 5 summarizes our results. We perform our ReLU with the SIMD circuits and activate all the 4096 packed data simultaneously. The offline time costs for circuit generation are 87.815ms and 100.143ms, respectively. The time consumptions in the online phase are 752.545ms and 516.413ms. The average per-data time costs of the offline and online computations are 0.045ms and 0.310ms.

Compared with the existing works using approximated polynomials, our GC-based circuits also provide higher efficiency. Table 6 illustrates the approximation polynomial with different degrees. For degree 6, the polynomial is $0.1249 + 0.5000x + 0.3729x^2 - 0.0410x^4 + 0.0016x^6$. Computing it takes 13 multiplications and 4 additions, which translates to 82.20ms. Our ReLU circuits thus outperform polynomial approximation by 265 times.

TABLE 7
Performance of each stage on the MNIST and CIFAR-10 datasets

	MNIST		CIFAR-10			
Phases	Stages	Latency (s)	Stages	Latency (s)	Stages	Latency (s)
Offline	$\mathcal{S}_1$	0.219	$\mathcal{S}_1$	3.711	–	–
	$\mathcal{S}_2$	0.252	$\mathcal{S}_2$	4.231	–	–
Online	1. Convolution	0.055	1. Convolution	0.425	10. Average Pooling	0.000
	2. ReLU Activation	0.425	2. ReLU Activation	20.304	11. Convolution	0.566
	3. Average Pooling	0.001	3. Convolution	9.062	12. ReLU Activation	1.268
	4. Convolution	0.098	4. ReLU Activation	20.304	13. Convolution	0.062
	5. ReLU Activation	0.317	5. Average Pooling	0.001	14. ReLU Activation	1.269
	6. Average Pooling	0.000	6. Convolution	2.266	15. Convolution	0.015
	7. Fully connected	0.006	7. ReLU Activation	5.075	16. ReLU Activation	0.317
	8. ReLU Activation	0.031	8. Convolution	2.265	17. Fully connected	0.002
	9. Fully connected	0.001	9. ReLU Activation	5.076	–	–
Total		3.835				76.224

TABLE 8
Performance of the synchronous and asynchronous computations on the MNIST and CIFAR-10 datasets

	MNIST dataset								CIFAR-10 dataset	
	Network 1		Network 2		Network 3		Network 4		Network 5	
	Syn. Comp	Asyn. Comp	Syn. Comp	Asyn. Comp	Syn. Comp	Asyn. Comp	Syn. Comp	Asyn. Comp	Syn. Comp	Asyn. Comp
Offline Phase (s)	0.007	0.005	0.020	0.016	0.052	0.050	0.471	0.469	7.946	7.845
Online Phase (s)	0.033	0.023	0.050	0.039	0.323	0.319	3.363	3.234	68.278	65.553
Total (s)	0.040	0.028	0.070	0.057	0.375	0.368	3.835	3.703	76.224	73.398

4.3.3 Evaluation on MNIST and CIFAR-10 dataset

Table 7 reports the latency for each stage of the network on the MNIST dataset (consists of 9 stages as presented in Fig. 7) and CIFAR-10 dataset (consists of 17 stages as described in Fig. 8). In the offline phase, the two servers interact with each other to prepare the triplets and the ReLU circuits, which costs 0.471s and 7.942s on the MNIST dataset and CIFAR-10 dataset. In the online phase, the activation function dominates since it uses garbled circuits. For the convolution layer, pooling layer, and fully connected layer, all the computations are executed over shares, which just takes a little time. Notably, for the client, encoding the query and decoding the prediction result just cost 5.568μs and 21.818μs on the MNIST dataset and CIFAR-10 dataset, respectively.

4.3.4 Evaluation on Different Network Architectures

We conduct experiment over network architectures in five published works [40], [25], [21], [23], which use a combination of FC and Conv layers as follows. For FC($784 \to 128$), 784 and 128 respectively represent the size of the input and the output. On the other hand, for Conv($1 \times 28 \times 28 \to 5 \times 13 \times 13$), the input image is of size 28×28 with 1 channel, the output image is of size

13×13 with 5 channels. For the square activation function, it is essentially multiplication operation between two secret shares. We can achieve this by using the triplet similar to the convolutional operation in our scheme.

- Network1 [40]: FC($784 \to 128$) $\Rightarrow$ Square $\Rightarrow$ FC($128 \to 128$) $\Rightarrow$ Square $\Rightarrow$ FC($128 \to 10$).
- Network2 [25]: Conv($1 \times 28 \times 28 \to 5 \times 13 \times 13$) $\Rightarrow$ ReLU $\Rightarrow$ FC($845 \to 100$) $\Rightarrow$ ReLU $\Rightarrow$ FC($100 \to 10$).
- Network3 [21]: Conv($1 \times 28 \times 28 \to 5 \times 13 \times 13$) $\Rightarrow$ Square $\Rightarrow$ Pooling($5 \times 13 \times 13 \to 5 \times 13 \times 13$) $\Rightarrow$ Conv ($5 \times 13 \times 13 \to 50 \times 5 \times 5$) $\Rightarrow$ Pooling($50 \times 5 \times 5 \to 50 \times 5 \times 5$) $\Rightarrow$ FC($1250 \to 100$) $\Rightarrow$ Square $\Rightarrow$ FC($100 \to 10$).
- Network4 [23]: the same as in Fig. 7.
- Network5 [23]: the same as in Fig. 8.

Table 8 shows the performance of synchronous and asynchronous computations in both the offline and online phases on the five networks. For network1, the total time cost of the existing schemes with synchronous computation is 0.040s, while the time cost of our scheme with asynchronous computation is just 0.028s. In other words, we obtain a 30.0 % performance saving. Analogously, the savings for network2, network3, network4, and network5 are 18.57%, 1.87%, 3.44%, and 3.71%, respectively. In short, our asynchronous computation reduces latency.
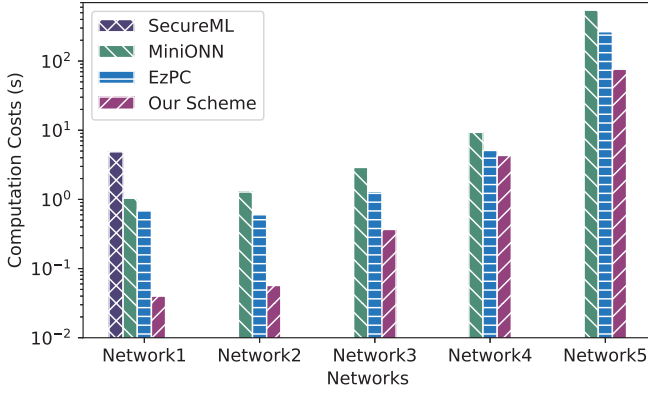
Fig. 12. Comparison of the computation overheads

Fig. 13. Comparison of the communication overheads

To demonstrate the superiority of our scheme, we compare with SecureML [40], MiniONN [23], and EzPC [27]. Fig. 12 and Fig. 13 show the computation and communication costs on different neural network architectures, respectively.

On the MNIST dataset (with Network1, 2, 3, 4), compared with MiniONN [23] (without model privacy), our scheme performs an average of $14.63\times$ and $36.69\times$ improvements on computation and communication costs, respectively. Compared with EzPC [27] (without model privacy), ours is $8.19\times$ and $31.32\times$ better on average (of Network1, 2, 3, 4) for the computation and communication costs, respectively. Compared with SecureML [40] (with model privacy) using Network1, we provide $122\times$ faster computation time and $1.09\times$ lower communication cost.

On the CIFAR dataset using Network5, our scheme achieves $7.14\times$ and $3.48\times$ improvements in reducing latency compared to MiniONN and EzPC. For the communication costs, our scheme outperforms MiniONN by $13.88\times$, and EzPC by $77.46\times$ times.

5 SECURITY ANALYSIS

Both the query and the model are randomly shared and distributed to two independent servers. As long as they do not collude, the privacy of the query and the model are preserved. More specifically, both servers always process them either over secret shares or over garbled circuits for non-linear activation, with the help of pre-computed triplets, which are independent of the sensitive data. So, no meaningful information is revealed to either of the servers.

Below we provide a simulation-based proof for security.

Security Definition: Let $f = (f_{\mathcal{U}}, f_{\mathcal{S}_1}, f_{\mathcal{S}_2})$ be a probabilistic polynomial function and $\prod$ a protocol computing f. The user and two servers want to compute $f(\mathcal{G}, \mathsf{C}^1, \mathsf{C}^2, \mathsf{W}^1, \mathsf{W}^2)$ using $\prod$ where $\mathcal{G}$ is the query image of the user $\mathcal{U}$, and $(\mathsf{C}^1, \mathsf{W}^1)$ and $(\mathsf{C}^2, \mathsf{W}^2)$ are the shared model deposited on the two servers. The view of $\mathcal{U}$ during the execution of $\prod$ is $V_{\mathcal{U}}(\mathcal{G}, \mathsf{C}^1, \mathsf{C}^2, \mathsf{W}^1, \mathsf{W}^2) = (\mathcal{G}, r_{\mathcal{U}}, m_{\mathcal{U}})$ where $r_{\mathcal{U}}$ is the random tape of $\mathcal{U}$, and m_U is the message received by $\mathcal{U}$. Simultaneously, the view of $\mathcal{S}_1$ and $\mathcal{S}_2$ are defined as $V_{\mathcal{S}_1}(\mathcal{G}, \mathsf{C}^1, \mathsf{C}^2, \mathsf{W}^1, \mathsf{W}^2) = (\mathsf{C}^1, \mathsf{W}^1, r_{\mathcal{S}_1}, m_{\mathcal{S}_1})$, $V_{\mathcal{S}_2}(a, b, c) = (\mathsf{C}^2, \mathsf{W}^2, r_{\mathcal{S}_2}, m_{\mathcal{S}_2})$. The protocol $\prod$ achieving the function f is regarded as secure if for every possible input $\mathcal{G}, \mathsf{C}^1, \mathsf{C}^2, \mathsf{W}^1, \mathsf{W}^2$ of f, there exist the probabilistic polynomial time simulators $\Phi_{\mathcal{U}}$, $\Phi_{\mathcal{S}_1}$, and $\Phi_{\mathcal{S}_2}$ such that,
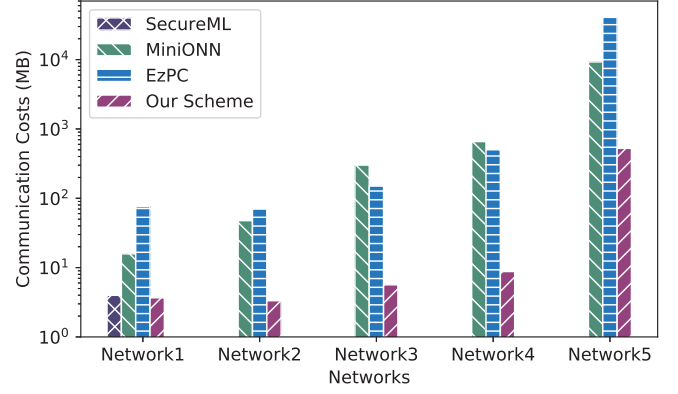
$$\Phi_{\mathcal{U}}(a, f_{\mathcal{U}}(\mathcal{G}, \mathsf{C}^1, \mathsf{C}^2, \mathsf{W}^1, \mathsf{W}^2)) \equiv_p V_{\mathcal{U}}(\mathcal{G}, \mathsf{C}^1, \mathsf{C}^2, \mathsf{W}^1, \mathsf{W}^2),$$
$$\Phi_{\mathcal{S}_1}(a, f_{\mathcal{S}_1}(\mathcal{G}, \mathsf{C}^1, \mathsf{C}^2, \mathsf{W}^1, \mathsf{W}^2)) \equiv_p V_{\mathcal{S}_1}(\mathcal{G}, \mathsf{C}^1, \mathsf{C}^2, \mathsf{W}^1, \mathsf{W}^2),$$
$$\Phi_{\mathcal{S}_2}(a, f_{\mathcal{S}_2}(\mathcal{G}, \mathsf{C}^1, \mathsf{C}^2, \mathsf{W}^1, \mathsf{W}^2)) \equiv_p V_{\mathcal{S}_2}(\mathcal{G}, \mathsf{C}^1, \mathsf{C}^2, \mathsf{W}^1, \mathsf{W}^2),$$

where $\equiv_p$ denotes computational indistinguishability.

Theorem 1: The triplet generation protocol in Section 3.2 is secure against semi-honest adversaries.

Proof: $\mathcal{S}_1$ holds the secret key. All the messages passed from $\mathcal{S}_1$ to $\mathcal{S}_2$ are encrypted. All those passed from $\mathcal{S}_2$ to $\mathcal{S}_1$ are distributed uniformly by adding random data independent of the data of $\mathcal{S}_2$. The view of $\mathcal{S}_1$ is $V_{\mathcal{S}_1} = (\mathsf{C}^1, \mathsf{W}^1, a_1, b_1, z_1)$, where a_1, b_1, z_1 come from the triplet of $\mathcal{S}_1$. We construct the simulator $\Phi_{\mathcal{S}_1}(\mathsf{C}^1, \mathsf{W}^1)$ as:

1) Pick the random integers $\hat{a}_1, \hat{b}_1, \hat{z}_1$ from $\mathbb{Z}_{2^t}$.
2) Output $\Phi_{\mathcal{S}_1}(\mathsf{C}^1, \mathsf{W}^1) = (\mathsf{C}^1, \mathsf{W}^1, \hat{a}_1, \hat{b}_1, \hat{z}_1)$.

As the randomness $\hat{a}_1$ (or $\hat{b}_1, \hat{z}_1$) is generated in the same manner as a_1 (or a_1, b_1), and independent from the other data, the distribution of $(\mathsf{C}^1, \mathsf{W}^1, \hat{a}_1, \hat{b}_1, \hat{z}_1)$ and $(\mathsf{C}^1, \mathsf{W}^1, a_1, b_1, z_1)$ are indistinguishable. Thus we have proven that $V_{\mathcal{S}_1} \equiv_p \Phi_{\mathcal{S}_1}(\mathsf{C}^1, \mathsf{W}^1)$. Analogously, $\Phi_{\mathcal{S}_2}(\mathsf{C}^2, \mathsf{W}^2) = (\mathsf{C}^2, \mathsf{W}^2, \hat{a}_2, \hat{b}_2, \hat{z}_2)$, $V_{\mathcal{S}_2} \equiv_p \Phi_{\mathcal{S}_2}(\mathsf{C}^2, \mathsf{W}^2)$.

Theorem 2: The query distribution protocol in Section 3.3.2 is secure against semi-honest adversaries.

Proof: User $\mathcal{U}$ additively shares the query image into two parts. The views of the three parties are $V_{\mathcal{U}} = (\mathcal{G}, R_{\mathcal{G}})$, $V_{\mathcal{S}_1} = (\mathsf{C}^1, \mathsf{W}^1, \mathcal{G}^1)$, $V_{\mathcal{S}_2} = (\mathsf{C}^2, \mathsf{W}^2, \mathcal{G}^2)$, where $\mathcal{G}^1 = R_{\mathcal{G}}$, $\mathcal{G}^2 = \mathcal{G} - R_{\mathcal{G}}$. We construct a simulator $\Phi_{\mathcal{S}_1}(\mathsf{C}^1, \mathsf{W}^1)$ as:

1) Pick random integers $\hat{R}_{\mathcal{G}}$ from $\mathbb{Z}_{2^t}$ and set $\hat{\mathcal{G}}^1 = \hat{R}_{\mathcal{G}}$.
2) Output $\Phi_{\mathcal{S}_1}(\mathsf{C}^1, \mathsf{W}^1) = (\mathsf{C}^1, \mathsf{W}^1, \hat{\mathcal{G}}^1)$.

Both $R_{\mathcal{G}}$ and $\hat{R}_{\mathcal{G}}$ are generated randomly. Hence the distribution of $R_{\mathcal{G}}$ and $\hat{R}_{\mathcal{G}}$ are indistinguishable. As a consequence, we have $V_{\mathcal{S}_1} \equiv_p \Phi_{\mathcal{S}_1}(\mathsf{C}^1, \mathsf{W}^1)$. Analogously, $\Phi_{\mathcal{S}_2}(\mathsf{C}^2, \mathsf{W}^2) = (\mathsf{C}^2, \mathsf{W}^2, \hat{\mathcal{G}}^2)$, $V_{\mathcal{S}_2} \equiv_p \Phi_{\mathcal{S}_2}(\mathsf{C}^2, \mathsf{W}^2)$.

Theorem 3: The convolutional computation protocol in Section 3.3.3 is secure against semi-honest adversaries.

Proof: The two servers perform the convolution with the help of triplets. Their views $V_{\mathcal{S}_1}$ and $V_{\mathcal{S}_2}$ are $(\mathsf{C}^1, \mathsf{W}^1, \mathcal{G}^1, \mathcal{H}^1, A_1, B_1, Z_1)$, $(\mathsf{C}^2, \mathsf{W}^2, \mathcal{G}^2, \mathcal{H}^2, A_1, B_1, Z_1)$ respectively. We construct a simulator $\Phi_{\mathcal{S}_1}(\mathsf{C}^1, \mathsf{W}^1)$ as:

1) Call the triplet generation protocol to have $\hat{A}_1, \hat{B}_1, \hat{Z}_1$.

2) Pick the random integers $\hat{\mathcal{G}}^1, \hat{U}^2, \hat{V}^2$ from $\mathbb{Z}_{2^t}$.

3) Compute $\hat{U} = \hat{\mathcal{G}}^1 - \hat{A}_1 + \hat{U}^2$, $\hat{V} = \mathsf{C}^1 - \hat{B}_1 + \hat{V}^2$.

4) Compute $\hat{\mathcal{H}}^1 = -\hat{U}\hat{V} + \hat{\mathcal{G}}^1\hat{V} + \mathsf{C}^1\hat{U} + \hat{Z}_1$.

5) Output $\Phi_{\mathcal{S}_1}(\mathsf{C}^1, \mathsf{W}^1) = (\mathsf{C}^1, \mathsf{W}^1, \hat{\mathcal{G}}^1, \hat{\mathcal{H}}^1)$.

The distribution of $\mathcal{H}^1$ and $\hat{\mathcal{H}}^1$ are indistinguishable. Hence $V_{\mathcal{S}_1} \equiv_p \Phi_{\mathcal{S}_1}(\mathsf{C}^1, \mathsf{W}^1)$ holds. Analogously, we have $\Phi_{\mathcal{S}_2}(\mathsf{C}^2, \mathsf{W}^2) = (\mathsf{C}^2, \mathsf{W}^2, \hat{\mathcal{G}}^2, \hat{\mathcal{H}}^2)$, and $V_{\mathcal{S}_2} \equiv_p \Phi_{\mathcal{S}_2}(\mathsf{C}^2, \mathsf{W}^2)$.

Theorem 4: The activation computation protocol in Section 3.3.4 is secure against semi-honest adversaries.

Proof: The two servers compute the activation function by using the designed garbled circuits. The view of $\mathcal{S}_1$ is $V_{\mathcal{S}_1} = (\mathsf{C}^1, \mathsf{W}^1, \mathcal{H}^1, \mathcal{J}^1)$. The view of $\mathcal{S}_2$ is $V_{\mathcal{S}_2} = (\mathsf{C}^2, \mathsf{W}^2, \mathcal{H}^2, \mathcal{J}^2)$. Since the garbled circuits are secure against semi-honest adversaries, we only consider the inputs and outputs of the circuits rather than the internal details. We construct a simulator $\Phi_{\mathcal{S}_1}(\mathsf{C}^1, \mathsf{W}^1)$ as:

1) Pick the random integers $\hat{\mathcal{H}}^1, \hat{\mathcal{J}}^1$ from $\mathbb{Z}_{2^t}$.

2) Output $\Phi_{\mathcal{S}_1}(\mathsf{C}^1, \mathsf{W}^1) = (\mathsf{C}^1, \mathsf{W}^1, \hat{\mathcal{H}}^1, \hat{\mathcal{J}}^1)$.

The distributions of $\mathcal{H}^1$ ($\mathcal{J}^1$) and $\mathcal{H}^1$ ($\hat{\mathcal{J}}^1$) are indistinguishable. Hence $V_{\mathcal{S}_1} \equiv_p \Phi_{\mathcal{S}_1}(\mathsf{C}^1, \mathsf{W}^1)$ holds. Analogously, we have $\Phi_{\mathcal{S}_2}(\mathsf{C}^2, \mathsf{W}^2) = (\mathsf{C}^2, \mathsf{W}^2, \hat{\mathcal{H}}^2, \hat{\mathcal{J}}^2)$, and $V_{\mathcal{S}_2} \equiv_p \Phi_{\mathcal{S}_2}(\mathsf{C}^2, \mathsf{W}^2)$.

Theorem 5: The pooling computation protocol in Section 3.3.5 is secure against semi-honest adversaries.

Proof: The view of $\mathcal{S}_1$ is $V_{\mathcal{S}_1} = (\mathsf{C}^1, \mathsf{W}^1, \mathcal{J}^1, \mathcal{K}^1)$. The view of $\mathcal{S}_2$ is $V_{\mathcal{S}_2} = (\mathsf{C}^2, \mathsf{W}^2, \mathcal{J}^2, \mathcal{K}^2)$. We construct a simulator $\Phi_{\mathcal{S}_1}(\mathsf{C}^1, \mathsf{W}^1)$ as:

1) Pick the random integers $\hat{\mathcal{J}}^1, \hat{\mathcal{K}}^1$ from $\mathbb{Z}_{2^t}$.

2) Output $\Phi_{\mathcal{S}_1}(\mathsf{C}^1, \mathsf{W}^1) = (\mathsf{C}^1, \mathsf{W}^1, \hat{\mathcal{J}}^1, \hat{\mathcal{K}}^1)$.

Since the distribution of $\mathcal{J}^1$ ($\mathcal{K}^1$) and $\mathcal{J}^1$ ($\hat{\mathcal{K}}^1$) are indistinguishable, $V_{\mathcal{S}_1} \equiv_p \Phi_{\mathcal{S}_1}(\mathsf{C}^1, \mathsf{W}^1)$ holds. Analogously, $\Phi_{\mathcal{S}_2}(\mathsf{C}^2, \mathsf{W}^2) = (\mathsf{C}^2, \mathsf{W}^2, \hat{\mathcal{J}}^2, \hat{\mathcal{K}}^2)$, and $V_{\mathcal{S}_2} \equiv_p \Phi_{\mathcal{S}_2}(\mathsf{C}^2, \mathsf{W}^2)$.

Theorem 6: The fully connected protocol in Section 3.3.6 is secure against semi-honest adversaries.

Proof: The views $V_{\mathcal{S}_1}$ and $V_{\mathcal{S}_2}$ are $(\mathsf{C}^1, \mathsf{W}^1, \mathcal{K}^1, \mathcal{F}^1, A_1, B_1, Z_1)$, $(\mathsf{C}^2, \mathsf{W}^2, \mathcal{K}^2, \mathcal{F}^2, A_2, B_2, Z_2)$ respectively. We construct a simulator $\Phi_{\mathcal{S}_1}(\mathsf{C}^1, \mathsf{W}^1)$ as:

1) Call the triplet generation protocol to have $\hat{A}_1, \hat{B}_1, \hat{Z}_1$.

2) Pick the random integers $\hat{\mathcal{K}}^1, \hat{U}^2, \hat{V}^2$ from $\mathbb{Z}_{2^t}$.

3) Compute $\hat{U} = \hat{\mathcal{K}}^1 - \hat{A}_1 + \hat{U}^2$, $\hat{V} = \mathsf{W}^1 - \hat{B}_1 + \hat{V}^2$.

4) Compute $\hat{\mathcal{F}}^1 = -\hat{U}\hat{V} + \hat{\mathcal{K}}^1\hat{V} + \mathsf{W}^1\hat{U} + \hat{Z}_1$.

5) Output $\Phi_{\mathcal{S}_1}(\mathsf{C}^1, \mathsf{W}^1) = (\mathsf{C}^1, \mathsf{W}^1, \hat{\mathcal{K}}^1, \hat{\mathcal{F}}^1)$.

The distribution of $\mathcal{F}^1$ and $\hat{\mathcal{F}}^1$ are indistinguishable. Hence $V_{\mathcal{S}_1} \equiv_p \Phi_{\mathcal{S}_1}(\mathsf{C}^1, \mathsf{W}^1)$ holds. Analogously, we have $\Phi_{\mathcal{S}_2}(\mathsf{C}^2, \mathsf{W}^2) = (\mathsf{C}^2, \mathsf{W}^2, \hat{\mathcal{K}}^2, \hat{\mathcal{F}}^2)$, and $V_{\mathcal{S}_2} \equiv_p \Phi_{\mathcal{S}_2}(\mathsf{C}^2, \mathsf{W}^2)$.

6 CONCLUSION AND FUTURE WORK

Neural-network prediction has unprecedented accuracy in many tasks, notably in image-based algorithms. However, privacy concerns have worried people when they hand in their data as a query. On the other hand, we see a growing market for machine learning model, the worry of model privacy is more pressing. We improve neural-network prediction in the secure outsourcing setting The privacy guarantees is that the servers providing the prediction service can get nothing about the query, the model, any intermediate results, and the final result. We design garbled circuits for non-linear activation function, which preserves the accuracy of the underlying neural network. We also reduce the overheads of computation and communication by adopting packing and asynchronous computation. Our experiments over both MNIST and CIFAR-10 datasets showcase our improvement.

As a very active research area, many works consider additional features. We discuss two limitations of our approach. Our scheme fails to provide verifiability, *i.e.*, the servers can deviate from the protocol specification and return wrong results. In critical applications, it is necessary to consider such possibility of malicious acts. Fortunately, the non-colluding assumption could be "fully leveraged" for achieving verifiability, specifically, by designing the corresponding maliciously-secure protocols, assuming more than two non-colluding servers [50].

Another limitation of our result is that we did not exploit GPU at all, despite its popularity in plaintext machine-learning. Some recent works integrate both SGX and GPU for prediction [18] and training [20]. Using the GPU to aid secure computation with SGX for training is already highly non-trivial [18], [20], using it to further improve cryptographic approaches would be a very interesting and challenging future direction.

REFERENCES

[1] I. Goodfellow, Y. Bengio, and A. Courville, *Deep Learning*. MIT Press, 2016, http://www.deeplearningbook.org.

[2] L. Zhao, Q. Wang, Q. Zou, Y. Zhang, and Y. Chen, "Privacy-preserving collaborative deep learning with unreliable participants," *IEEE Trans. Information Forensics and Security*, vol. 15, pp. 1486–1500, 2020.

[3] Q. Zou, Y. Wang, Q. Wang, Y. Zhao, and Q. Li, "Deep learning-based gait recognition using smartphones in the wild," *IEEE Trans. Information Forensics and Security*, vol. 15, pp. 3197–3212, 2020.

[4] Q. Zou, H. Jiang, Q. Dai, Y. Yue, L. Chen, and Q. Wang, "Robust lane detection from continuous driving scenes using deep neural networks," *IEEE Trans. Veh. Technol.*, vol. 69, no. 1, pp. 41–54, 2020.

[5] F. Tramèr, F. Zhang, A. Juels, M. K. Reiter, and T. Ristenpart, "Stealing machine learning models via prediction APIs," in *USENIX Security Symposium*, 2016, pp. 601–618.

[6] Y. Adi, C. Baum, M. Cissé, B. Pinkas, and J. Keshet, "Turning your weakness into a strength: Watermarking deep neural networks by backdooring," in *USENIX Security Symposium*, 2018, pp. 1615–1631.

[7] R. Shokri, M. Stronati, C. Song, and V. Shmatikov, "Membership inference attacks against machine learning models," in *IEEE Symposium on Security and Privacy (S&P)*, 2017, pp. 3–18.

[8] J. Hayes, L. Melis, G. Danezis, and E. D. Cristofaro, "LOGAN: membership inference attacks against generative models," *PoPETs*, vol. 2019, no. 1, pp. 133–152, 2019.

[9] A. Salem, Y. Zhang, M. Humbert, P. Berrang, M. Fritz, and M. Backes, "ML-Leaks: Model and data independent membership inference attacks and defenses on machine learning models," in *ISOC Network and Distributed System Security Symposium (NDSS)*, 2019.

[10] N. Papernot, P. D. McDaniel, I. J. Goodfellow, S. Jha, Z. B. Celik, and A. Swami, "Practical black-box attacks against machine learning," in *ACM Asia Conference on Computer and Communications Security (AsiaCCS)*, 2017, pp. 506–519.

[11] J. Jia and N. Z. Gong, "AttriGuard: A practical defense against attribute inference attacks via adversarial machine learning," in *USENIX Security Symposium*, 2018, pp. 513–529.

[12] G. F. Elsayed, S. Shankar, B. Cheung, N. Papernot, A. Kurakin, I. J. Goodfellow, and J. Sohl-Dickstein, "Adversarial examples that fool both computer vision and time-limited humans," in *Neural Information Processing Systems (NeurIPS)*, 2018, pp. 3914–3924.

[13] Z. Wang, M. Song, S. Zheng, Z. Zhang, Y. Song, and Q. Wang, "Invisible adversarial attack against deep neural networks: An adaptive penalization approach," *IEEE Trans. Dependable Sec. Comput.*, 2019, DOI: 10.1109/TDSC.2019.2929047.

[14] M. Abadi, A. Chu, I. J. Goodfellow, H. B. McMahan, I. Mironov, K. Talwar, and L. Zhang, "Deep learning with differential privacy," in *ACM Conference on Computer and Communications Security (CCS)*, 2016, pp. 308–318.

[15] A. D. Smith, A. Thakurta, and J. Upadhyay, "Is interaction necessary for distributed private learning?" in *IEEE Symposium on Security and Privacy (S&P)*, 2017, pp. 58–77.

[16] O. Ohrimenko, F. Schuster, C. Fournet, A. Mehta, S. Nowozin, K. Vaswani, and M. Costa, "Oblivious multi-party machine learning on trusted processors," in *USENIX Security Symposium*, 2016, pp. 619–636.

[17] S. Hu, L. Y. Zhang, Q. Wang, Z. Qin, and C. Wang, "Towards private and scalable cross-media retrieval," *IEEE Trans. Dependable Sec. Comput.*, 2019, DOI: 10.1109/TDSC.2019.2926968.

[18] F. Tramèr and D. Boneh, "Slalom: Fast, verifiable and private execution of neural networks in trusted hardware," in *International Conference on Learning Representations (ICLR)*, 2019.

[19] S. S. M. Chow, "Can we securely outsource big data analytics with lightweight cryptography?" in *International Workshop on Security in Cloud Computing, SCC@ASIACCS*, 2019, p. 1.

[20] L. K. L. Ng, S. S. M. Chow, A. P. Y. Woo, D. P. H. Wong, and Y. Zhao, "Goten: GPU-outsourcing trusted execution of neural network training and prediction," 2019.

[21] R. Gilad-Bachrach, N. Dowlin, K. Laine, K. E. Lauter, M. Naehrig, and J. Wernsing, "CryptoNets: Applying neural networks to encrypted data with high throughput and accuracy," in *International Conference on Machine Learning (ICML)*. ACM, 2016, pp. 201–210.

[22] H. Chabanne, A. de Wargny, J. Milgram, C. Morel, and E. Prouff, "Privacy-preserving classification on deep neural network," IACR Cryptology ePrint Archive 2017/035, 2017.

[23] J. Liu, M. Juuti, Y. Lu, and N. Asokan, "Oblivious neural network predictions via MiniONN transformations," in *ACM Conference on Computer and Communications Security (CCS)*, 2017, pp. 619–631.

[24] C. Juvekar, V. Vaikuntanathan, and A. Chandrakasan, "GAZELLE: A low latency framework for secure neural network inference," in *USENIX Security Symposium*, 2018, pp. 1651–1669.

[25] B. D. Rouhani, M. S. Riazi, and F. Koushanfar, "DeepSecure: scalable provably-secure deep learning," in *Design Automation Conference (DAC)*, 2018, pp. 2:1–2:6.

[26] M. S. Riazi, M. Samragh, H. Chen, K. Laine, K. E. Lauter, and F. Koushanfar, "XONN: XNOR-based oblivious deep neural network inference," in *USENIX Security Symposium*, 2019, pp. 1501–1518.

[27] N. Chandran, D. Gupta, A. Rastogi, R. Sharma, and S. Tripathi, "EzPC: Programmable, efficient, and scalable secure two-party computation," in *EuroS&P*. IEEE, 2019, pp. 496–511.

[28] C. Gentry, "Fully homomorphic encryption using ideal lattices," in *Symposium on Theory of Computing (STOC)*. ACM, 2009, pp. 169–178.

[29] R. Bost, R. A. Popa, S. Tu, and S. Goldwasser, "Machine learning classification over encrypted data," in *ISOC Network and Distributed System Security Symposium (NDSS)*, 2015.

[30] R. K. H. Tai, J. P. K. Ma, Y. Zhao, and S. S. M. Chow, "Privacy-preserving decision trees evaluation via linear functions," in *European Symposium on Research in Computer Security (ESORICS)*, 2017, pp. 494–512.

[31] A. Aloufi, P. Hu, H. W. H. Wong, and S. S. M. Chow, "Blindfolded evaluation of random forests with multi-key homomorphic encryption," *IEEE Trans. Dependable Sec. Comput.*, 2019, DOI: 10.1109/TDSC.2019.2940020.

[32] S. S. M. Chow, "Privacy-preserving machine learning (Invited paper)," in *Frontiers in Cyber Security. FCS 2018*, ser. Communications in Computer and Information Science, vol. 879. Springer, 2018.

[33] E. Hesamifard, H. Takabi, M. Ghasemi, and R. N. Wright, "Privacy-preserving machine learning as a service," *PoPETs*, vol. 2018, no. 3, pp. 123–142, 2018.

[34] X. Jiang, M. Kim, K. E. Lauter, and Y. Song, "Secure outsourced matrix computation and application to neural networks," in *ACM Conference on Computer and Communications Security (CCS)*, 2018, pp. 1209–1222.

[35] S. S. M. Chow, J. Lee, and L. Subramanian, "Two-party computation model for privacy-preserving queries over distributed databases," in *ISOC Network and Distributed System Security Symposium (NDSS)*, 2009.

[36] S. Kamara, P. Mohassel, and M. Raykova, "Outsourcing multi-party computation," IACR Cryptology ePrint Archive 2011/272.

[37] B. Wang, M. Li, S. S. M. Chow, and H. Li, "A tale of two clouds: Computing on data encrypted under multiple keys," in *IEEE Conference on Communications and Network Security, CNS*, 2014, pp. 337–345.

[38] M. Baryalai, J. Jang-Jaccard, and D. Liu, "Towards privacy-preserving classification in neural networks," in *Privacy, Security and Trust (PST)*, 2016, pp. 392–399.

[39] Q. Wang, M. Du, X. Chen, Y. Chen, P. Zhou, X. Chen, and X. Huang, "Privacy-preserving collaborative model learning: The case of word vector training," *IEEE Trans. Knowl. Data Eng.*, vol. 30, no. 12, pp. 2381–2393, 2018.

[40] P. Mohassel and Y. Zhang, "SecureML: A system for scalable privacy-preserving machine learning," in *IEEE Symposium on Security and Privacy (S&P)*. IEEE, 2017, pp. 19–38.

[41] A. Shamir, "How to share a secret," *Commun. ACM*, vol. 22, no. 11, pp. 612–613, 1979.

[42] D. Beaver, "Efficient multiparty protocols using circuit randomization," in *Advances in Cryptology – CRYPTO*, 1991, pp. 420–432.

[43] A. C. Yao, "How to generate and exchange secrets," in *IEEE Symposium on Foundations of Computer Science*. IEEE, 1986, pp. 162–167.

[44] N. P. Smart and F. Vercauteren, "Fully homomorphic SIMD operations," *Des. Codes Cryptography*, vol. 71, no. 1, pp. 57–81, 2014.

[45] D. Demmler, T. Schneider, and M. Zohner, "ABY - A framework for efficient mixed-protocol secure two-party computation," in *ISOC Network and Distributed System Security Symposium (NDSS)*, 2015.

[46] J. W. Bos, K. E. Lauter, J. Loftus, and M. Naehrig, "Improved security for a ring-based fully homomorphic encryption scheme," in *IMA Int'l Conference on Cryptography and Coding (IMACC)*, 2013, pp. 45–64.

[47] N. Dowlin, R. Gilad-Bachrach, K. Laine, K. E. Lauter, M. Naehrig, and J. Wernsing, "Manual for using homomorphic encryption for bioinformatics," *Proc. of the IEEE*, vol. 105, no. 3, pp. 552–567, 2017.

[48] Y. LeCun, "The MNIST database of handwritten digits," http://yann.lecun.com/exdb/mnist, 1998.

[49] A. Krizhevsky and G. Hinton, "Learning multiple layers of features from tiny images," Tech. Rep., 2009.

[50] P. Mohassel and P. Rindal, "ABY³: A mixed protocol framework for machine learning," in *ACM Conference on Computer and Communications Security (CCS)*. ACM, 2018, pp. 35–52.

APPENDIX

FURTHER ILLUSTRATION

Here we provide two supplementary illustrations for our triplet generation protocol in the offline phase. Fig. 14 (left) illustrates the existing synchronous design. Our asynchronous design, which keeps the servers busy with the remaining operations that do not involve feedback from the other, is illustrated in Fig. 14 (right) Finally, Fig. 15 illustrates a toy example for the packed triplet generation.
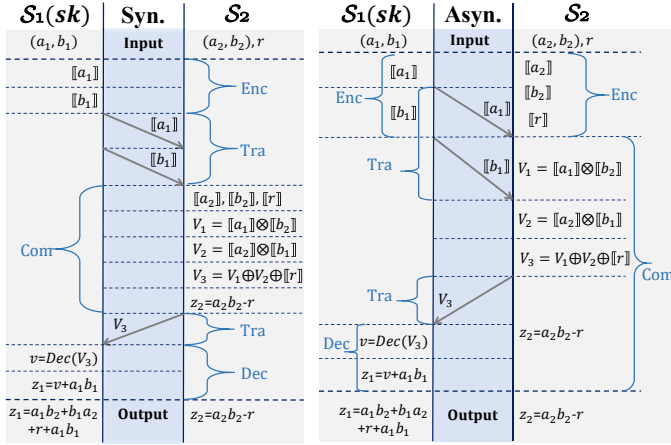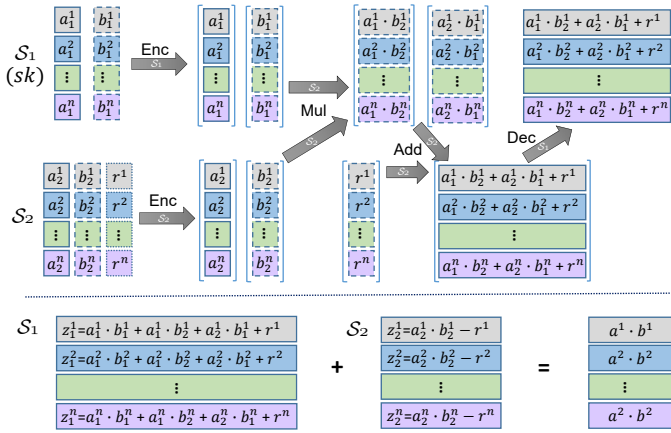

Fig. 14. Synchronous/Asynchronous computations

Fig. 15. A toy example of simultaneous triplet generation for 4 triplets